

Supporting Information

on

**Exploring supercapacitance of solvothermally synthesized N-rGO sheet: Role
of N-doping and the insight mechanism**

Ankit Yadav[†], Rajeev Kumar[†] and Balaram Sahoo^{}*

Materials Research Centre, Indian Institute of Science, Bangalore-560012, India

[†]Authors contributed equally

ORCID IDs:

Ankit Yadav - 0000-0002-2239-8000

Rajeev Kumar- 0000-0002-5436-2352

Balaram Sahoo - 0000-0002-2050-4746

**Corresponding author's email: bsahoo@iisc.ac.in*

Tel no.: +91-8022932943

S1. Materials and Method

The chemicals used for the synthesis of GO sheets and N-rGO are flake graphite powder (Sigma Aldrich), H₂SO₄ (98% GR, Merck), conc. HCl (35.4%, SDFCL), KMnO₄ (99%, Qualigens), H₃PO₄ (Sigma Aldrich), acetone (≥99.5%, EMPLURA), H₂O₂ (30%, Merck), Urea and N-N-dimethylformamide (DMF).

S1.1 Instrument

The structural morphology of the N-rGO samples was inspected by a *Scanning Electron Microscope* (SEM). X-Ray Diffraction (XRD) patterns were recorded using a *PANalytical X-ray diffractometer* (operated at 40 kV and 150 mA) in a 2θ range from 10° to 55° (Cu-K_α radiation, λ = 1.540 Å). Raman spectra were recorded on *LabRam HR* equipment (532 nm laser source). The nitrogen doping and relative amounts of oxygen and nitrogen-containing functionalities were estimated through X-ray Photoelectron spectroscopy (XPS) analysis. XPS study was performed on K-Alpha spectrometer having a monochromated X-ray source (Al K_α) with a spot size of 400 μm. The hemispherical analyzer was maneuvered with an energy of 200 eV in a constant analyzer energy mode.

S1.2 Electrode preparation and electrochemical testing methods

The electrochemical measurements were performed for all the samples using a BIOLOGIC Potentiostat/Galvanostat (SP-200) both in 3-electrode as well as 2-electrode configuration. Aqueous (0.5 M) H₂SO₄ was used as an electrolyte. Nitrogen gas was purged prior to all electrochemical measurements at room temperature. In the 3-electrode system, a glassy carbon electrode was used as a working electrode, Ag/AgCl (3.5 M KCl) as the reference electrode, and Pt mesh as the counter electrode. The area of the glassy

carbon electrode was 0.07 cm^2 . For the working electrode preparation for 3-electrode measurement, typically, 2 mg of the sample was well mixed in 500 μl ethanol and sonicated for 15 minutes for homogenization. 2.5 μl Nafion (5% solution in isopropyl alcohol (IPA)) was added and again sonicated for 15 minutes. As electrode area was small, 5 μl of this dispersion was deposited on a glassy carbon electrode, as use in earlier report ^{1,2} and dried for 30 minutes at room temperature. For the 2-electrode system, N-rGO-3 sample and Polyvinylidene difluoride (PVDF, binder) were taken in a ratio of 95:5 along with minute droplets of N-Methyl-2-Pyrrolidone (NMP) to prepare an ink. The ink was deposited on two carbon cloth pieces ($1 \times 1 \text{ cm}^2$). The final loading on each piece was approximately 2.0 mg sample after drying. The two pieces were then sandwiched with a separator (PTFE) and wetted with a few drops of 0.5 M H_2SO_4 . The sandwiched structure was then assembled in a Swagelok cell.

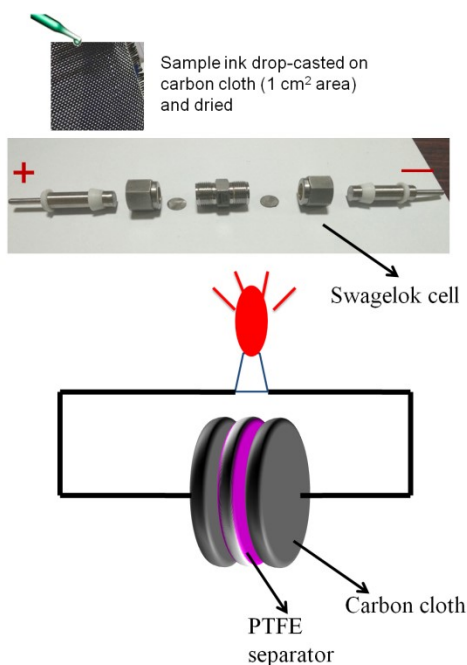


Figure S1. The schematics of preparation of symmetric 2 electrode device.

Electrochemical studies like cyclic voltammetry (CV), galvanostatic charge-discharge (GCD) and electrochemical impedance spectroscopy (EIS) measurements were carried out in 0.5 M H₂SO₄ aqueous solution as the electrolyte. The potential was swept in the range from 0.0 to 0.8 V (versus Ag/AgCl) at the scan rates of 5,10, 20, 50 and 100 mV/s. EIS investigations were performed in the frequency range of 200 KHz to 10 mHz at room temperature using a voltage amplitude of 5 mV. The GCD experiments were performed at several current densities (mass normalized currents) from 0.5 A/g to 10 A/g in the constant potential window of 0.0 V to 0.8 V. The areal capacitance values from the CV curves are obtained through equation (S1) for 3 electrode system ³:

$$C_{Areal} = \frac{\int IdV}{A \times v \times \Delta V} \quad (S1)$$

where ‘I’ denotes the current value in the CV curve, ΔV represents the voltage window, ‘v’ is the potential scanning rate and ‘A’ is the surface area of the single electrode (in cm²).

Furthermore, The specific capacitance (C_{sp}) values from the GCD curves are measured in Farad per gram and calculated using the equation (S2) for 3 electrode system ³.

$$C_{sp} = \frac{I \times \Delta t}{m \times \Delta V} \quad (S2)$$

Here, ‘I’ is the constant implemented current in mA, ‘Δt’ is discharge time in seconds, ‘m’ is the mass in mg of the sample used on the active electrode surface area and ‘ΔV’ is the potential difference between the initial and final potential.

S1.2.1 Calculation of specific capacitance based on galvanostatic charge discharge curves for 2 electrode symmetric device

For 2 electrode **symmetric** cell configuration specific capacitance derived from GCD curves can be calculated from the equation ⁴⁻⁶

$$C_{sp} = \frac{4 \times I \times \Delta t}{m \times \Delta V} \quad (S3)$$

here, 'I' is the constant implemented current in mA, 'Δt' is discharge time in seconds, 'm' is the mass in mg of the sample used on the active electrode surface area and 'ΔV' is potential difference between initial and final potential.

Energy density (E) and power density (P) derived from galvanostatic experiment can be calculated from the following equations:

$$E_D = \frac{C_{sp} \times \Delta V^2 \times 1000}{8 \times 3600} \quad (S4)$$

$$P_D = \frac{E_D \times 3600}{\Delta t} \quad (S5)$$

where E, C, ΔV, P and Δt are the specific energy, specific capacitance, potential window, specific power and discharge time, respectively.

S1. Characterization

S1.1 SEM images

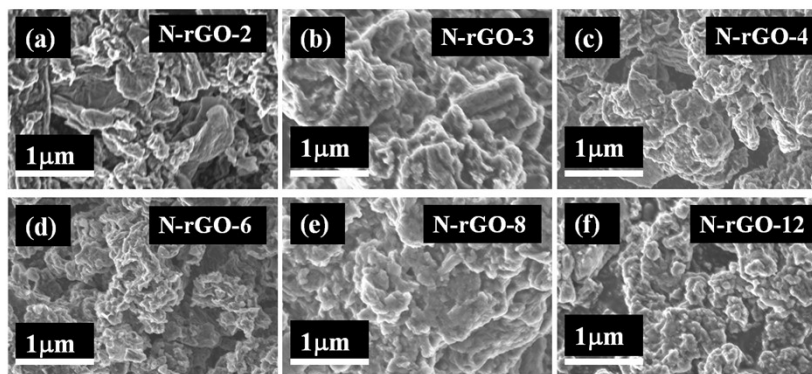


Figure S2.The SEM images of all the synthesized N-rGO samples, as indicated.

S1.3 Crystallite size and Average crystallite size calculated from XRD data using Debye-Scherrer's equation

Scherrer's equation S6 is ⁷ :

$$L_c = \frac{K\lambda}{\beta \cos\theta} \quad (S6)$$

Where,

L_c = crystallites size (nm)

K = 0.9 (Scherrer constant)

λ = 0.15406 nm (wavelength of the x-ray sources)

β = Full width at half maximum (FWHM)(radians))

θ = Peak position (radians)

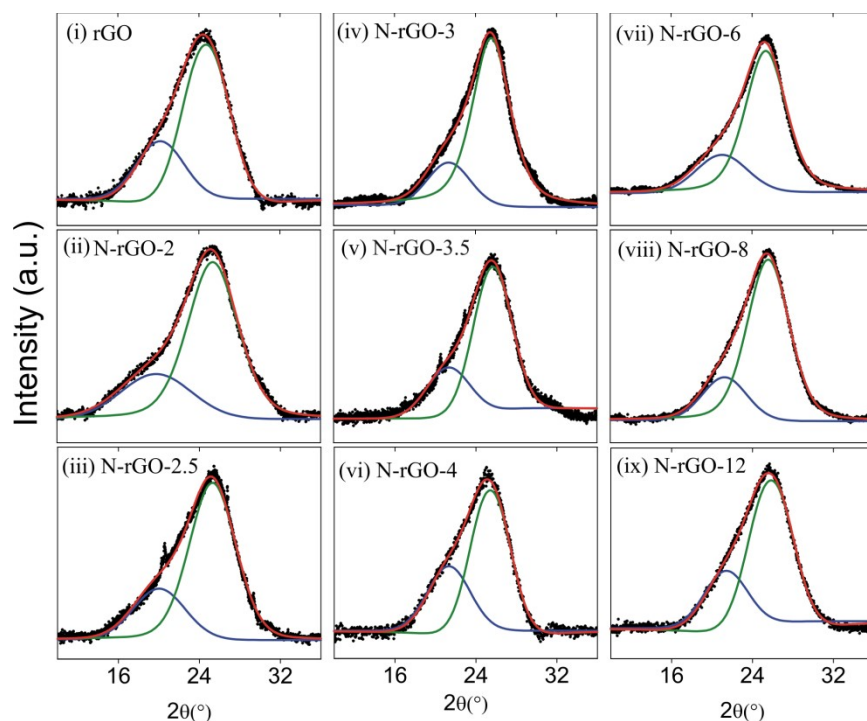


Figure S3. Fitted XRD (002) peak of synthesized rGO and N-rGO samples, as indicated.

Table S1. Crystallites size of N-rGO samples obtained using Scherrer's equation and the (002) Bragg peak. (FWHM = Full width at half maximum, L_c = Crystallite size).

Sample	Peak 1				Peak 2			
	2θ	FWHM (β)	Area (%)	L_c (nm)	2θ	FWHM (β)	Area (%)	L_c (nm)
rGO	20.1	5.92	34	1.46	24.7	5.26	66	1.54
N-rGO-2	19.7	8.16	26	0.98	25.3	5.88	74	1.38
N-rGO-2.5	20.0	5.99	25	1.34	25.2	5.43	75	1.49
N-rGO-3	21.3	4.88	19	1.65	25.5	4.34	81	1.87
N-rGO-3.5	21.3	5.01	28	1.61	25.6	4.47	72	1.81
N-rGO-4	21.3	4.94	36	1.63	25.0	4.52	64	1.79
N-rGO-6	21.1	5.90	22	1.36	25.3	4.79	78	1.69
N-rGO-8	21.2	5.09	20	1.58	25.6	4.91	80	1.65
N-rGO-12	21.1	4.04	28	1.60	25.7	4.99	72	1.63

For the purpose of obtaining detailed insights into the supercapacitive mechanism in our synthesized samples, we also calculated the average crystallites size (L_c) (it can also represent the thickness of the flakes/sheets) using Debye-Scherrer's equation (eq. S6, Supporting Information) through the fitting of the (002) Bragg peak of the XRD patterns of the N-rGO samples. The (002) diffraction peak for each sample is fitted with two sub-peaks, a sub-peak (peak 1) at lower 2θ corresponding to highly disorder/amorphous like rGO and a sub-peak (peak 2) at higher 2θ corresponding to the better crystalline rGO sheets. The fitted (002) peak for all the samples is shown in Figure S3 (Supporting Information) and the results are given in Table 2. There is a trend of a decrease in full width at half maximum (FWHM) of peak 1 for all the N-rGO samples. Along with the highly amorphous regions of the rGO/N-rGO sheets, this peak (peak 1) may correspond to the regions of improper reduction too. Anyway, the area under the peak 1 is only a minor part in comparison to peak 2, which represents to the major volume of the sample. Hence, from here on, we consider the peak 2. From the results listed in Table 2, we observe that the rGO sample has a larger crystallite size than N-rGO-2 sample. To understand this, one may consider the nature of the GO sheets after reduction through the solvothermal process in the presence of 2 g of urea. It will be clear later that the N-rGO samples have doped nitrogen in their graphene-like sheets. This nitrogen comes from urea, which is used to reduce the GO sheets to rGO by the solvothermal process. It is demonstrated that after N-doping, the defects in the graphene-like rGO sheets increases³⁴, which leads to an *improper* stacking of the exfoliated graphene sheets. This improper stacking of these defected graphene sheets (during the process of drying) is observed as the origin of line-broadening of the (002) XRD peak for N-rGO-2 sample. Hence, even with a small amount of N-doping, the ordering is not favored and the crystallite size is less for N-rGO-2 in comparison to rGO sample.

It can also be noticed from Table 2 that the peak 2 for the rGO sample is observed at a lower 2θ value (24.7°) than all other samples, signifying a slightly higher average interlayer separation than the other samples. This implies that a complete/proper reduction of GO has not happened in the rGO sample; this can be due to the fact that this sample was synthesized without using any reducing agent (urea) during the solvothermal process. With increasing the amount of the reducing agent (urea), i.e., for the samples synthesized using a higher amount of urea (please keep in mind that the amount of GO was always fixed at 1 g and the amount of solvent was also fixed to 80 ml in a 100 ml autoclave), the crystallite size increases till 3 g of urea, i.e., for N-rGO-3 sample. Beyond this amount of urea, the crystallinity/crystallite size of the samples decreases continuously. From table 2, this can be understood that as the amount of reducing agent (urea content) increases, the reduction (from GO to rGO) becomes better. However, due to the availability of more nitrogen, too much nitrogen is doped in the rGO sheets, which makes the samples more defective/amorphous-like and the FWHM of the (002) peak becomes large, i.e., crystallite size decreases continuously. The presence of more nitrogen in the samples prepared using more than 3 g of urea will be demonstrated later through the XPS results.

S1.3. Electrochemical Study

3-electrode system CV measurements were done using glassy carbon electrode (area 0.07 cm^2) with different scan rates to record the voltammograms. Galvanostatic charge discharge (GCD) curves were recorded at different current densities with sample deposition of $5\mu\text{l}$ and $0.5\text{ M H}_2\text{SO}_4$ as electrolyte.

S1.3.1 CV and GCD graphs of GO, rGO and N-doped reduced graphene oxide (N-rGO) samples at different scan rates and different current densities

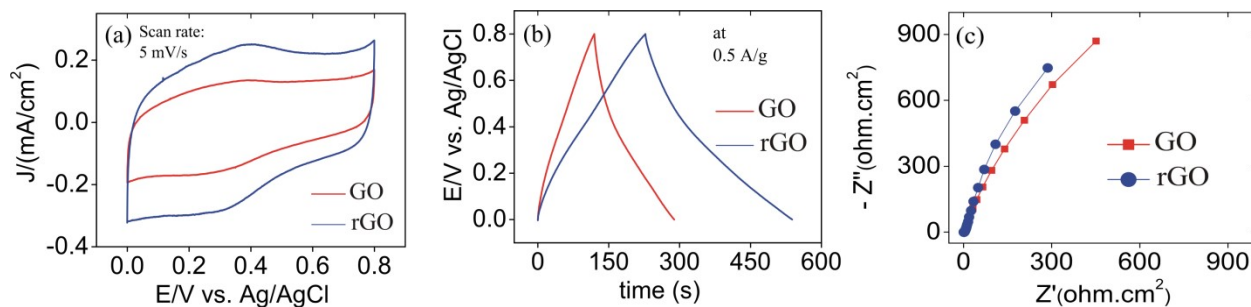


Figure S4. Electrochemical measurements using a 3-electrode system: (a) cyclic voltammograms of GO and rGO samples at 5 mV/s scan rate. (b) GCD plots of GO and rGO samples at 0.5 A/g current density. (c) Nyquist plots of GO and rGO samples.

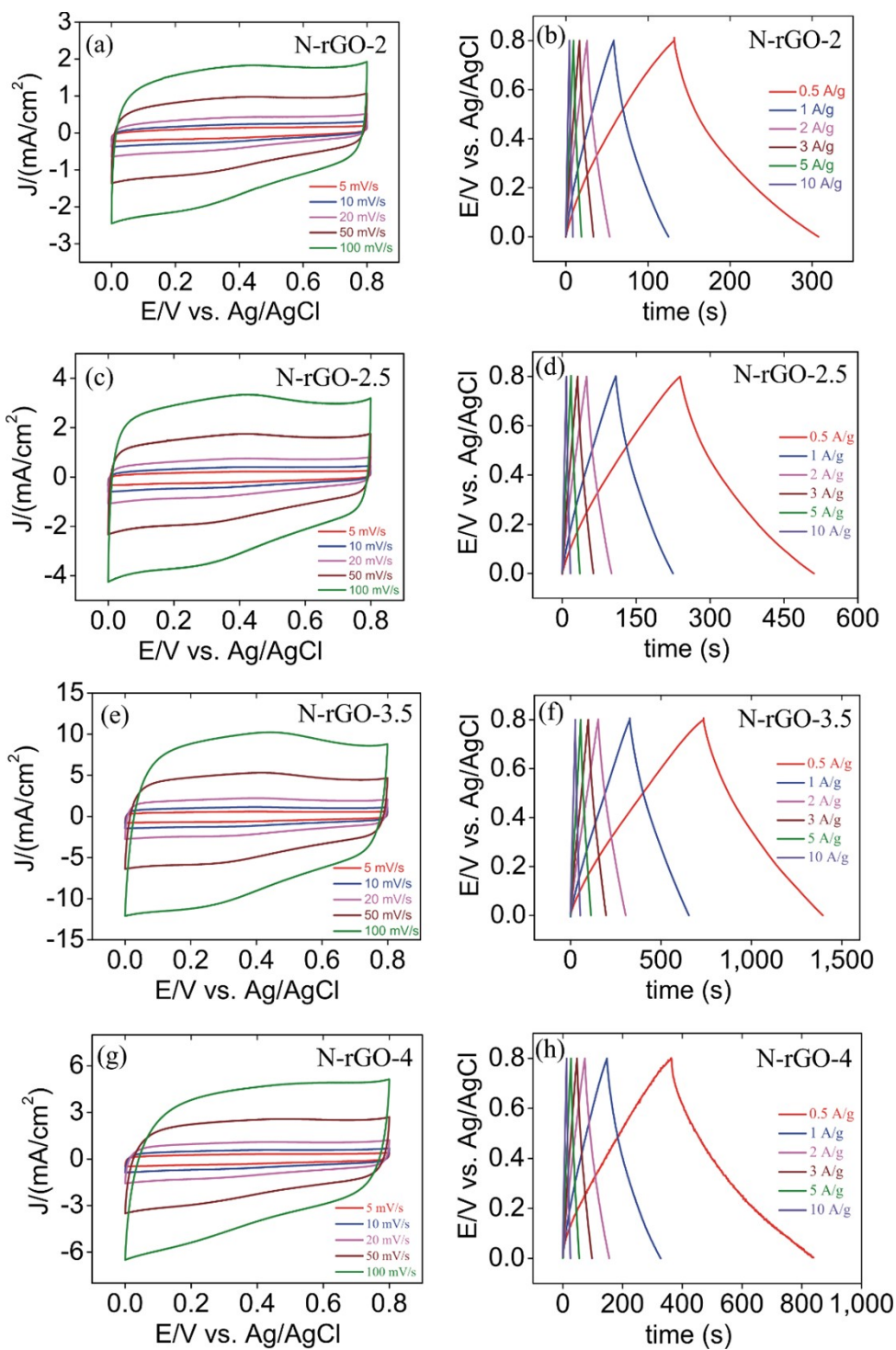


Figure S5. (a,c,e,g) Cyclic voltammograms at different scan rates. (b,d,f,h) GCD plots at different current densities for N-rGO-2, N-rGO-2.5, N-rGO-3.5 and N-rGO-4 samples.

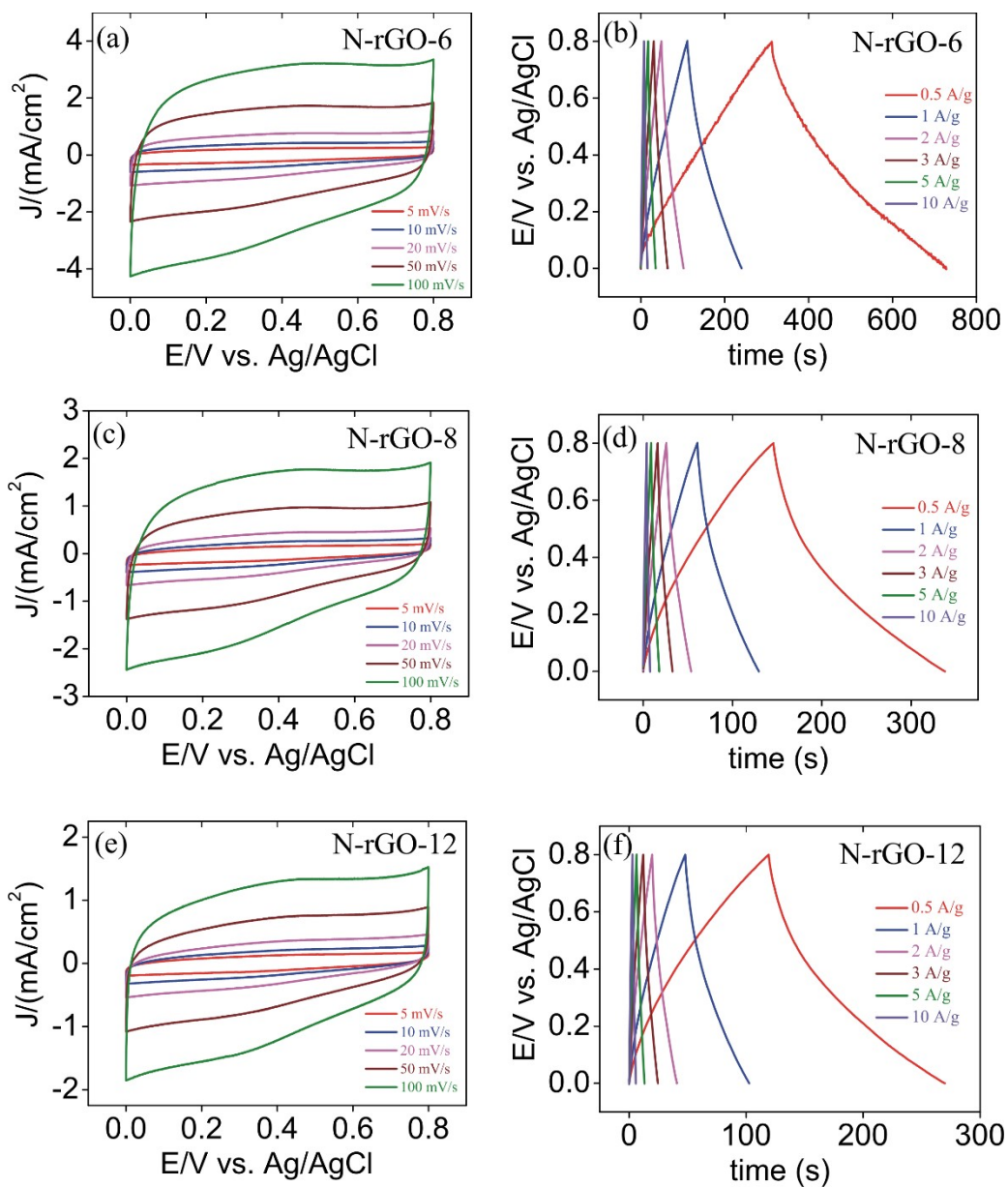


Figure S6. (a,c,e) Cyclic voltammograms at different scan rates for N-rGO-6, N-rGO-8 and N-rGO-12 samples. (b,d,f) GCD plots at different current densities for N-rGO-6, N-rGO-8 and N-rGO-12 samples.

S1.3.2 Nyquist plot of N-rGO samples

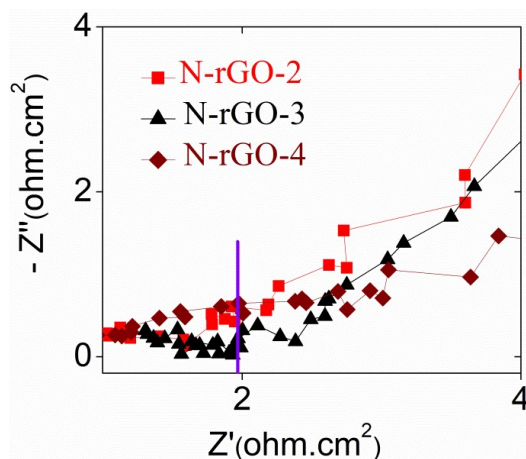


Figure S7. Zoomed-in Nyquist plot of N-rGO samples.

S1.4 Determination of crystallite size and number of graphene layers from Raman spectra

From the fitted Raman spectra we determined the number of layers through the general equation

⁸: L_a was calculated using Tuinstra-Koenig Eq. S7 ⁸

$$L_a = (2.4 \times 10^{-10}) (\lambda^4) (I_D / I_G)^{-1} \quad (S7)$$

where, $\lambda = 532$ nm (used wavelength). Earlier, researchers illustrated that the thickness of monolayer graphene is 0.335 nm and the thickness of the bilayer, triple layer, four-layer, and seven-layer graphene is 0.81, 1.285, 1.76, and 3.185 nm ⁹, respectively. In Table S2 we observed that rGO has more number of layers than any other N-rGO samples. The possible reason may be because of incomplete exfoliation and as a result rGO remains relatively thick with more number of layers. But in N-rGO-2 sample the reduction improves along with higher exfoliation.

Table S2. Crystallite size (L_a) of N-rGO samples obtained from Raman spectra.

Sample Name	I_G/I_D	L_a (nm)	No. of layers
GO	0.15	3.0	9.1
rGO	0.21	4.2	12.5
N-rGO-2	0.15	3.0	8.9
N-rGO-3	0.16	3.1	9.3
N-rGO-4	0.17	3.3	10.0
N-rGO-6	0.18	3.4	10.3
N-rGO-8	0.18	3.5	10.5
N-rGO-12	0.20	3.8	11.5

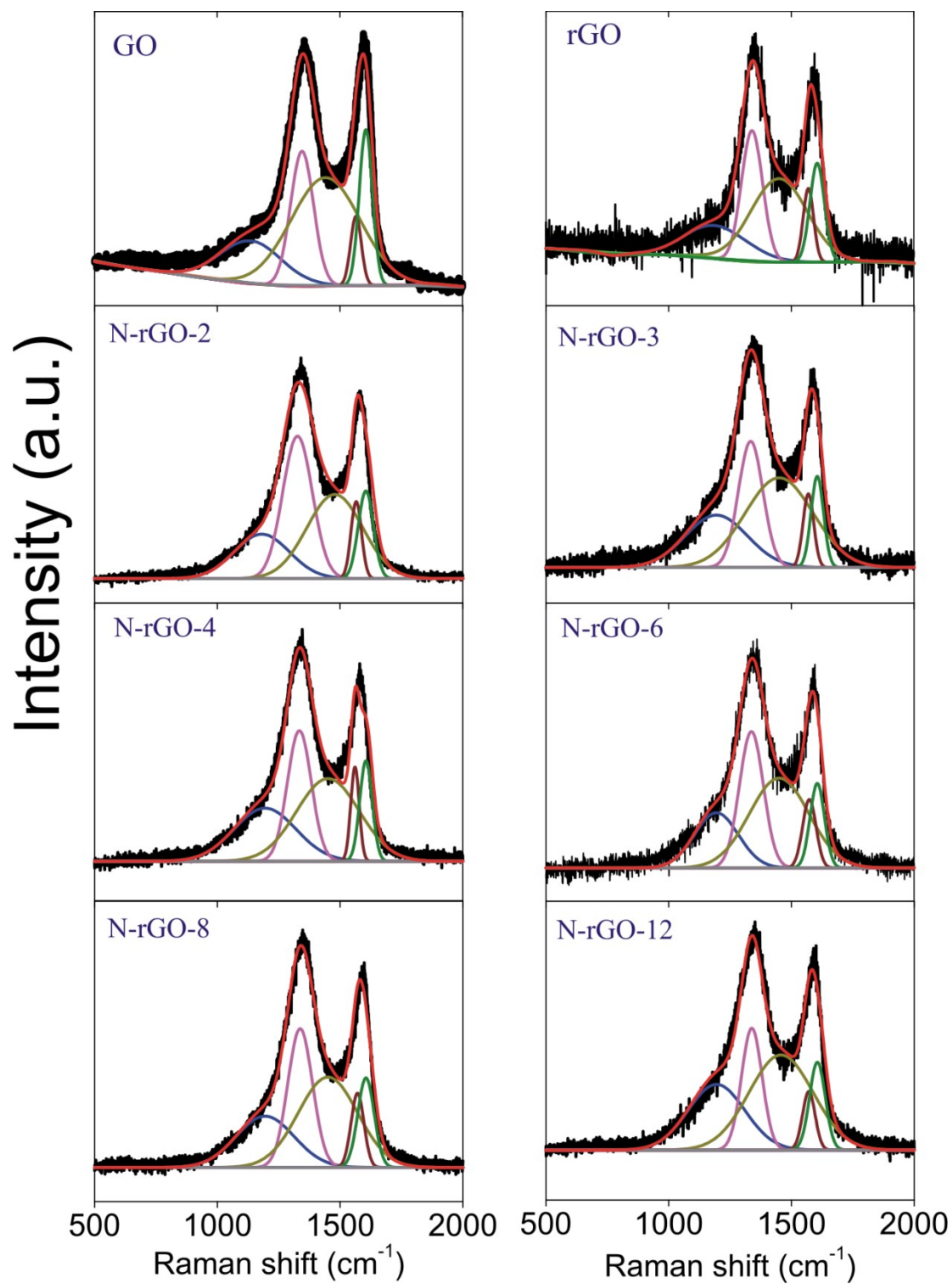


Figure S8. Fitted Raman spectra of the synthesized GO, rGO and N-rGO samples, as indicated.

S1.5 XPS spectra of GO and rGO

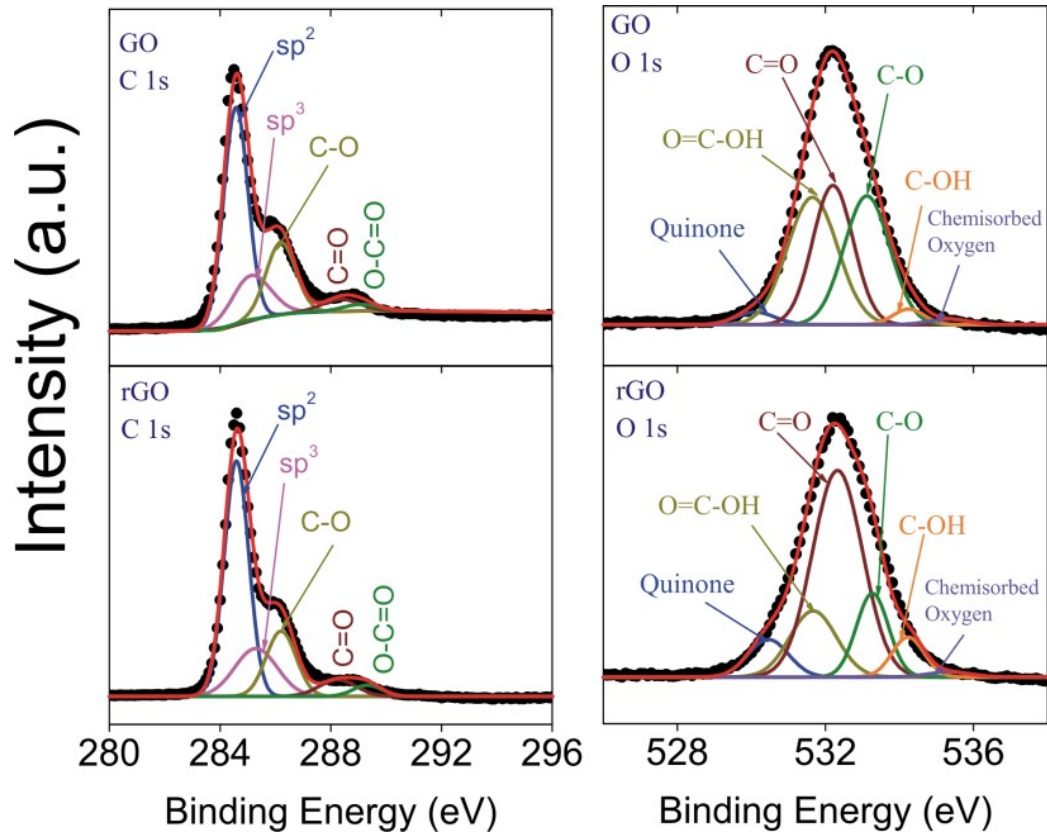


Figure S9. XPS spectra of GO, rGO - C1s (left panel) and O1s (right panel).

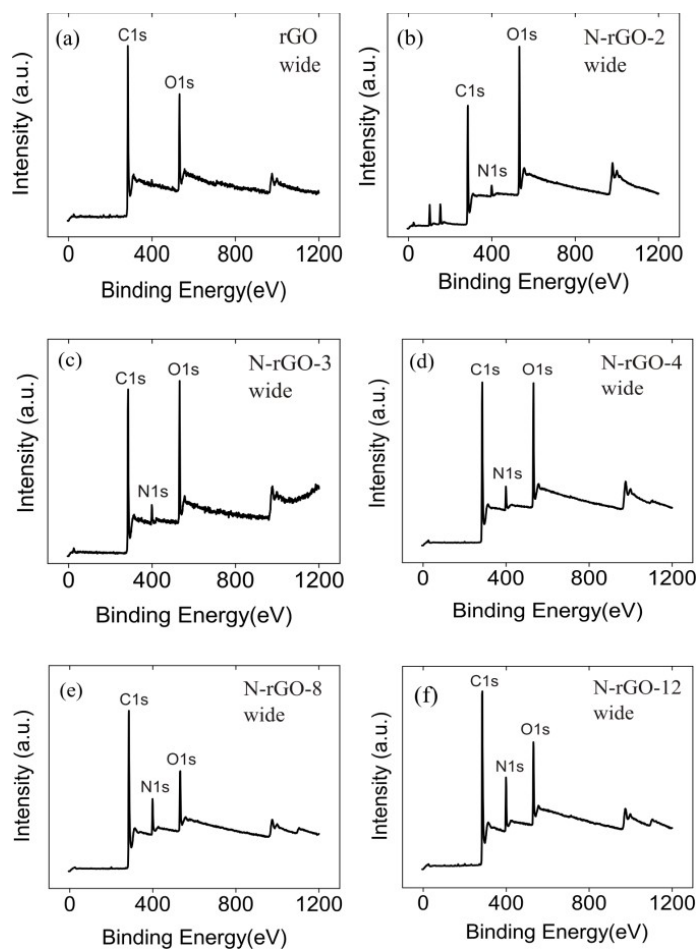


Figure S10. The XPS spectra of the synthesized samples in the full measured energy range.

Table S3. C1s XPS spectral parameters for GO and rGO samples.

Sample		C-C (sp ²) (eV)	C-C (sp ³) (eV)	C-OH (eV)	C-O-C (eV)	O=C-OH/ O=C-NH (eV)
GO	Position	284.5	285.1	286.1	288.3	289.0
	Area (%)	54	17	21	5	3
rGO	Position	284.5	285.2	286.2	288.2	289.3
	Area (%)	54	19	18	6	3

Table S4. O1s XPS spectral parameters for GO and rGO samples.

Sample		Quinone (eV)	O=C-OH (eV)	C=O (eV)	C-O (eV)	C-OH (eV)	Chemisorbed Oxygen (eV)
GO	Position	530.1	531.6	532.2	533.1	534.2	535.3
	Area (%)	2	33	29	31	3	1
rGO	Position	530.4	531.6	532.3	533.2	534.2	535.3
	Area (%)	8	16	54	14	7	1

Table S5. O1s XPS spectral parameters for N-rGO samples.

Sample		Quinone (eV)	N-O (eV)	O=C-OH (eV)	C=O (eV)	C-O (eV)	C-OH (eV)	Chemisorbed Oxygen (eV)
N-rGO-2	Position	530.10	531.18	531.65	532.41	533.13	534.04	535.32
	Area (%)	1	7	9	43	29	10	0.82
N-rGO-3	Position	530.10	531.10	531.65	532.47	533.10	534.01	535.34
	Area (%)	3	5	6	49	26	10	0.91
N-rGO-4	Position	530.11	531.10	531.60	532.31	533.18	534.00	535.32
	Area (%)	4	11	7	44	25	8	0.75
N-rGO-8	Position	530.19	531.14	531.61	532.34	533.16	534.02	535.34
	Area (%)	1	10	8	24	24	19	14
N-rGO-12	Position	530.17	531.19	531.65	532.30	533.13	534.09	535.31
	Area (%)	1	11	11	34	20	21	2

Table S6. The C 1s XPS spectral parameters for all the N-rGO samples.

Sample		C-C	C-C	C-N/ C-OH	C-O-C	O=C-OH/ O=C-NH
		(sp ²) (eV)	(sp ³) (eV)	(eV)	(eV)	(eV)
N-rGO-2	Position	284.55	285.34	286.24	288.43	289.56
	Area (%)	46	22	26	4	2
N-rGO-3	Position	284.68	285.29	286.33	288.35	289.50
	Area (%)	33	16	45	3	3
N-rGO-4	Position	284.70	285.28	286.16	288.19	289.50
	Area (%)	36	28	27	7	2
N-rGO-8	Position	284.63	285.28	286.30	288.25	289.56
	Area (%)	48	18	21	11	2
N-rGO-12	Position	284.59	285.15	286.43	288.60	289.51
	Area (%)	35	31	25	5	4

S1.6 BET specific surface area study

Table S7. Calculated specific surface area, total pore volume and mean pore diameter values of NrGO-3 and N-rGO-8

Samples	Specific Surface area (m ² /g)	Total pore volume (cm ³ /g)	Mean Pore diameter (nm)
N-rGO-3	324	0.220	2.721
N-rGO-8	50	0.0560	4.527

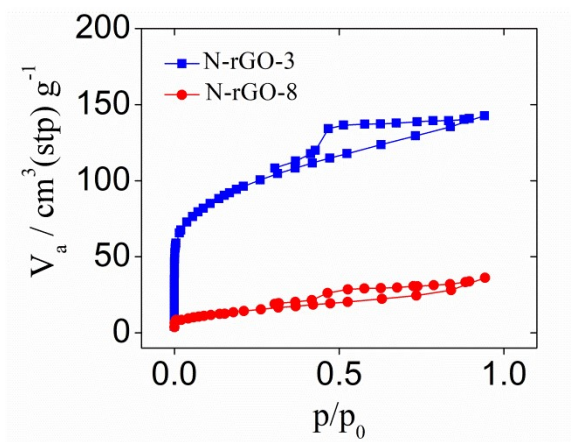


Figure S11. N₂ adsorption/desorption isotherm and BET surface area value of N-rGO-3 and N-rGO-8.

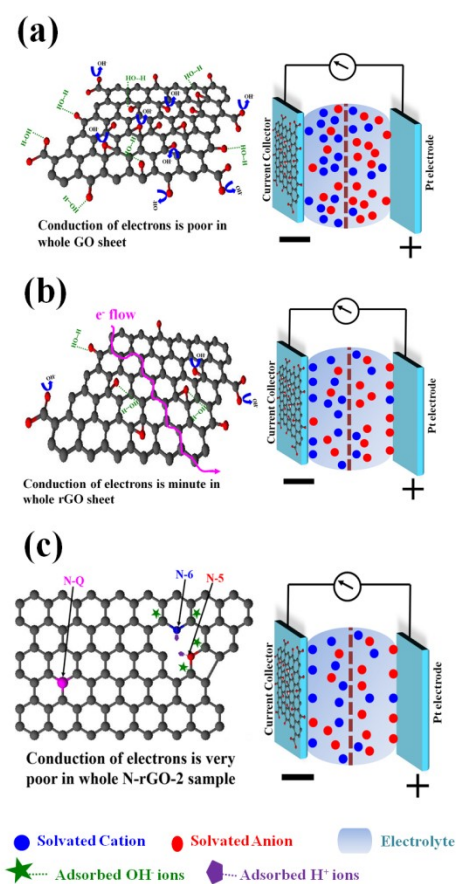


Figure S12. Pictorial representation of the mechanistic insights of adsorption of active ions on the electrode of different types of synthesized samples: (a) GO (b) rGO and (c) N-rGO-2.

S1.7 Comparison with previous literature reports

Table S8. Literature reports on the amount of N-doping (at %), synthesis method and specific capacitance (C_{sp}) value for N-rGO sample.

S.No.	Atomic % of N	Synthesis Method	C_{sp} (F/g)	Ref
1.	~1	Hydrothermal	246	10
2.	~7.7	Solvothermal	301	11
3.	~8.62	Hydrothermal	161	3
4.	~12.75	Solvothermal	170	12
5.	~2.77	Hydrothermal	194	13
6.	~3.2	Thermally exfoliated	82	14
7.	~5.96	Chemical	244	15
8.	~9.6	Thermally exfoliation	248	16
9.	~3	Hydrothermal	218	17
10.	~10.13	Hydrothermal	326	18
11.	~10.9-13.4	Hydrothermal	244	19
12.	~2-10	Hydrothermal	218	20
13.	~10	Hydrothermal	300	21
14.	~6.85	Hydrothermal	242	22
15.	~ 5.74	Solvothermal	514	Present Work

References

- 1 M. Saraf, K. Natarajan, S. M. Mobin, K. Natarajan and S. M. Mobin, Robust Nanocomposite of Nitrogen-Doped Reduced Graphene Oxide and MnO₂ Nanorods for High-Performance Supercapacitors and Nonenzymatic Peroxide Sensors, *ACS Sustain. Chem. Eng.*, 2018, **6**, 10489–10504.
- 2 H. Nolan, B. Mendoza-Sanchez, N. Ashok Kumar, N. McEvoy, S. O'Brien, V. Nicolosi and G. S. Duesberg, Nitrogen-doped reduced graphene oxide electrodes for electrochemical supercapacitors, *Phys. Chem. Chem. Phys.*, 2014, **16**, 2280–2284.
- 3 J. W. Lee, J. M. Ko and J. D. Kim, Hydrothermal preparation of nitrogen-doped graphene sheets via hexamethylenetetramine for application as supercapacitor electrodes, *Electrochim. Acta*, 2012, **85**, 459–466.

- 4 Z. J. Zhang, D. H. Xie, P. Cui and X. Y. Chen, Conversion of a zinc salicylate complex into porous carbons through a template carbonization process as a superior electrode material for supercapacitors, *RSC Adv.*, 2014, **4**, 6664–6671.
- 5 A. R. Thiruppathi, B. Sidhureddy, M. Salverda, P. C. Wood and A. Chen, Novel three-dimensional N-doped interconnected reduced graphene oxide with superb capacitance for energy storage, *J. Electroanal. Chem.*, 2020, **875**, 113911 (1–9).
- 6 J. Yang, M. R. Jo, M. Kang, Y. S. Huh, H. Jung and Y. M. Kang, Rapid and controllable synthesis of nitrogen doped reduced graphene oxide using microwave-assisted hydrothermal reaction for high power-density supercapacitors, *Carbon N. Y.*, 2014, **73**, 106–113.
- 7 M. Pawlyta, J. N. Rouzaud and S. Duber, Raman microspectroscopy characterization of carbon blacks: Spectral analysis and structural information, *Carbon N. Y.*, 2015, **84**, 479–490.
- 8 L. G. Cañado, K. Takai, T. Enoki, M. Endo, Y. A. Kim, H. Mizusaki, A. Jorio, L. N. Coelho, R. Magalhães-Paniago and M. A. Pimenta, General equation for the determination of the crystallite size l_a of nanographite by Raman spectroscopy, *Appl. Phys. Lett.*, 2006, **88**, 1–4.
- 9 S. Ye, H. Huang, C. Yuan, F. Liu, M. Zhai, X. Shi, C. Qi and G. Wang, Thickness-dependent strain effect on the deformation of the graphene-encapsulated Au nanoparticles, *J. Nanomater.*, 2014, **2014**, 1–6.
- 10 T. Wang, L. Wang, D. Wu, W. Xia, H. Zhao and D. Jia, Hydrothermal synthesis of nitrogen-doped graphene hydrogels using amino acids with different acidities as doping agents, *J. Mater. Chem. A*, 2014, **2**, 8352–8361.
- 11 Y. Lu, F. Zhang, T. Zhang, K. Leng, L. Zhang, X. Yang, Y. Ma, Y. Huang, M. Zhang and Y. Chen, Synthesis and supercapacitor performance studies of N-doped graphene materials using o-phenylenediamine as the double-N precursor, *Carbon N. Y.*, 2013, **63**, 508–516.
- 12 H. M. Jeong, J. W. Lee, W. H. Shin, Y. J. Choi, H. J. Shin, J. K. Kang and J. W. Choi, Nitrogen-doped graphene for high-performance ultracapacitors and the importance of nitrogen-doped sites at basal planes, *Nano Lett.*, 2011, **11**, 2472–2477.
- 13 F. M. Hassan, V. Chabot, J. Li, B. K. Kim, L. Ricardez-Sandoval and A. Yu, Pyrrolic-structure enriched nitrogen doped graphene for highly efficient next generation supercapacitors, *J. Mater. Chem. A*, 2013, **1**, 2904–2912.
- 14 C. Wang, Y. Zhou, L. Sun, Q. Zhao, X. Zhang, P. Wan and J. Qiu, N/P-Codoped thermally reduced graphene for high-performance supercapacitor applications, *J. Phys. Chem. C*, 2013, **117**, 14912–14919.
- 15 P. Wang, H. He, X. Xu and Y. Jin, Significantly enhancing supercapacitive performance of nitrogen-doped graphene nanosheet electrodes by phosphoric acid activation, *ACS*

- Appl. Mater. Interfaces*, 2014, **6**, 1563–1568.
- 16 Z. Wen, X. Wang, S. Mao, Z. Bo, H. Kim, S. Cui, G. Lu, X. Feng and J. Chen, Crumpled nitrogen-doped graphene nanosheets with ultrahigh pore volume for high-performance supercapacitor, *Adv. Mater.*, 2012, **24**, 5610–5616.
 - 17 Y. H. Lee, K. H. Chang and C. C. Hu, Differentiate the pseudocapacitance and double-layer capacitance contributions for nitrogen-doped reduced graphene oxide in acidic and alkaline electrolytes, *J. Power Sources*, 2013, **227**, 300–308.
 - 18 L. Sun, L. Wang, C. Tian, T. Tan, Y. Xie, K. Shi, M. Li and H. Fu, Nitrogen-doped graphene with high nitrogen level via a one-step hydrothermal reaction of graphene oxide with urea for superior capacitive energy storage, *RSC Adv.*, 2012, **2**, 4498–4506.
 - 19 A. Śliwak, B. Grzyb, N. Diez and G. Gryglewicz, Nitrogen-doped reduced graphene oxide as electrode material for high rate supercapacitors, *Appl. Surf. Sci.*, 2017, **399**, 265–271.
 - 20 L. Lai, L. Chen, D. Zhan, L. Sun, J. Liu, S. H. Lim, C. K. Poh, Z. Shen and J. Lin, One-step synthesis of NH₂-graphene from in situ graphene-oxide reduction and its improved electrochemical properties, *Carbon N. Y.*, 2011, **49**, 3250–3257.
 - 21 X. Fan, C. Yu, J. Yang, Z. Ling and J. Qiu, Hydrothermal synthesis and activation of graphene-incorporated nitrogen-rich carbon composite for high-performance supercapacitors, *Carbon N. Y.*, 2014, **70**, 130–141.
 - 22 D. Wang, Y. Min, Y. Yu and B. Peng, A general approach for fabrication of nitrogen-doped graphene sheets and its application in supercapacitors, *J. Colloid Interface Sci.*, 2014, **417**, 270–277.